
Article:
Olivieri, DA, Fairweather, M and Falle, SAEG (2010) Adaptive mesh refinement applied to the scalar transported PDF equation in a turbulent jet. International Journal for Numerical Methods in Engineering, 84 (4). pp. 434-447. ISSN 0029-5981

https://doi.org/10.1002/nme.2899

Adaptive Mesh Refinement Applied to the Scalar Transported PDF Equation in a Turbulent Jet

D.A. Olivieri[1,*], M. Fairweather[1] and S.A.E.G. Falle[2]

[1]School of Process, Environmental and Materials Engineering, The University of Leeds, Leeds LS2 9JT, U.K.
[2]School of Mathematics, The University of Leeds, Leeds LS2 9JT, U.K.
*d.a.olivieri@leeds.ac.uk

Summary

This paper describes a novel solution method for the transported probability density function (PDF) equation for scalars (compositions). In contrast to conventional solution methods based on the Monte Carlo approach, we use a finite-volume method combined with adaptive mesh refinement (AMR) applied in both physical and compositional space. The obvious advantage of this over a uniform grid is that fine meshes are only used where the solution requires high resolution. The efficiency of the method is demonstrated by a number of tests involving a turbulent jet flow with up to two scalars (both reacting and non-reacting). We find that the AMR calculation can be at a fraction of the computer cost of a uniform grid calculation with the same accuracy.

Keywords: transported PDF; adaptive mesh refinement; finite-volume method; Reynolds-averaged Navier-Stokes; molecular mixing

1. Introduction

Transported PDF methods are currently the most promising and rigorous means for linking turbulent flow calculations with finite-rate chemistry. In principle, they can be used to provide a complete statistical description of a turbulent flow field by modelling the PDF for both the velocity and scalar fields [1]. In this paper, our aims are somewhat rather less ambitious: we merely consider the scalar PDF for the mixing and reaction of scalars in a turbulent jet flow.

It is well known that finite-difference or finite-volume methods are viable for the transported PDF equation solution on a uniform grid for simple flows with a small number of scalars (e.g. [2]), but the computational cost becomes prohibitive as the number of variables increases. Pope [1] estimates that the cost increases exponentially with the number of scalars, whereas it is claimed that it only increases linearly with the number of scalars for the Monte Carlo methods. It is for this reason that all current solution methods for the PDF transport equation are based on the Monte Carlo techniques.

However, Sabel'nikov and Soulard [3] have carried out a detailed review of all current Monte Carlo methods used in the simulation of turbulent reacting flows and compared them with finite-difference methods on uniform grids. They found that the exponential rise in CPU time with the number of scalars applies equally to both the Monte Carlo and the finite-difference method, if one insists on maintaining the same accuracy as the number of scalars increases. In a previous paper [4], we also found this to be true for both the adaptive mesh refinement (AMR) and the Monte Carlo method applied to compositional space alone. This means that PDF methods can strictly only be applied to practical reacting flow situations involving large numbers of chemical species if they are combined with methods that reduce the complexity of the chemistry. For example, the intrinsic low-dimensional manifold approach [5] is known to be capable of giving good predictions of flames with relatively complex chemistry while requiring only a small number of species in the computations. Other methods for reducing the complexity of the chemistry are available, e.g. species lumping approaches [6] and the computational singular perturbation method [7].

In this paper, we consider an alternative solution technique for the joint-scalar PDF equation that uses the AMR in both physical and compositional space to improve the efficiency of a finite-volume method. The fact that the PDF only differs significantly from zero in a small

fraction of compositional space means that the computational cost for AMR is much smaller than for a uniform grid. This, combined with the saving due to adaptive refinement in physical space, means that the computational cost is much less than for a uniform grid, as used by Janicka et al. [2]. Since the technique proposed is a finite-volume method, it can also be readily combined with the majority of current computational fluid dynamics codes.

AMR is now a well-established technique. The earliest applications were to two-dimensional shock problems [8, 9]. Later extensions include three-dimensional problems [10] and implementation on parallel machines [11]. The advantage of AMR is that it can use error estimates to adaptively increase grid resolution to meet accuracy requirements in specific parts of the computational domain. AMR offers particular advantages for transient problems with traveling discontinuities such as shocks. In some classes of problems, CPU and memory requirements can be reduced over those for a uniform grid by as much as a factor of one hundred [12].

2. Governing Equations

2.1. The PDF equation

Consider a reacting system of N chemical species with concentrations ω_α ($\alpha = 1, \ldots, N$) that satisfy the reaction equations

$$\frac{\mathrm{d}\omega_\alpha}{\mathrm{d}t} = S_\alpha(\omega_1, \ldots, \omega_N), \tag{1}$$

where S_α is the rate of reaction $\dot{\omega}_\alpha$ for specie α. From [1] the evolution of the mass-weighted probability $P(\mathbf{r}, \omega_1 \ldots \omega_N; t)$ is given by

$$\rho\frac{\partial}{\partial t}P + \rho\tilde{u_k}\frac{\partial}{\partial x_k}P + \rho\sum_{\alpha=1}^{N}\frac{\partial}{\partial\omega_\alpha}(S_\alpha P) = \frac{\partial}{\partial x_k}\frac{\mu}{\sigma_p}\frac{\partial P}{\partial x_k} + \rho\left(\frac{\partial P}{\partial t}\right)_{\mathrm{mm}}. \tag{2}$$

Here u_k is the mean velocity, μ is the turbulent viscosity and σ_p is the Prandtl number for the turbulent diffusion of P. The superscript tilde denotes density-weighted averaging.

The last term in (2) represents molecular mixing, for which there are a number of models. The simplest is the linear mean square estimation (LMSE) method in which

$$\left(\frac{\partial P}{\partial t}\right)_{\mathrm{mm}} = -\sum_{\alpha=1}^{N}\frac{\partial}{\partial\omega_\alpha}\left[\frac{\varepsilon C_D}{2k}(\omega_\alpha - \langle\omega_\alpha\rangle)P\right]. \tag{3}$$

Here C_D, ε and k are the ratio of the scalar to mechanical turbulent time scales, the viscous dissipation rate of turbulence kinetic energy and the turbulence kinetic energy per unit mass (see [1] for details).

There are other possibilities for this term: the coalescence/dispersion or the Curl model [13] and the Langevin model [1]. However, the Curl model is expensive since it involves an integro-differential equation and, as we showed in [4], it does not give realistic results. The Langevin model would be applicable except that it is not possible to impose conditions at the boundaries of compositional space that ensure that the mean and variance behave in the correct way. We shall therefore adopt the LMSE model [14, 15] herein.

2.2. The flow equations

The flow is computed from the mass and momentum conversation equations for turbulent flow using a standard k–ε turbulence model with a thin shear layer approximation in cylindrical symmetry with the parabolic approximation for steady flow [16]. It is assumed that the

turbulence is statistically two-dimensional, stationary, axisymmetric and non-swirling. The equations are

$$\begin{aligned}
&\frac{\partial(\rho\tilde{u})}{\partial z}+\frac{1}{r}\frac{\partial(r\rho\tilde{v})}{\partial r}=0,\\
&\rho\tilde{u}\frac{\partial\tilde{u}}{\partial z}+\rho\tilde{v}\frac{\partial\tilde{u}}{\partial r}=\frac{1}{r}\frac{\partial}{\partial r}r\mu\frac{\partial\tilde{u}}{\partial r},\\
&\rho\tilde{u}\frac{\partial k}{\partial z}+\rho\tilde{v}\frac{\partial k}{\partial r}=\frac{1}{r}\frac{\partial}{\partial r}r\frac{\mu}{\sigma_k}\frac{\partial k}{\partial r}+\mu\left(\frac{\partial\tilde{u}}{\partial r}\right)^2-\rho\varepsilon,\\
&\rho\tilde{u}\frac{\partial\varepsilon}{\partial z}+\rho\tilde{v}\frac{\partial\varepsilon}{\partial r}=\frac{1}{r}\frac{\partial}{\partial r}r\frac{\mu}{\sigma_\varepsilon}\frac{\partial\varepsilon}{\partial r}+\frac{\varepsilon}{k}\left[\mu C_{\varepsilon 1}\left(\frac{\partial\tilde{u}}{\partial r}\right)^2-C_{\varepsilon 2}\rho\varepsilon\right].
\end{aligned}\tag{4}$$

Here $\tilde{u}$, $\tilde{v}$ are the mean velocities in the *z* and *r* directions, and σ_k, σ_ε are the Prandtl numbers for *k* and ε. Owing to the thin shear layer approximation, only the $\tilde{u}$ -component of the momentum equation has been given. The turbulent viscosity is given by the usual expression

$$\mu=\rho C_\mu\frac{k^2}{\varepsilon}.\tag{5}$$

We assume that the pressure is constant, which avoids the need for a Poissson solver. As we shall see in Section 4, this is a good approximation for such flows. The continuity equation is unnecessary since the density can be calculated from the mass fractions ω_α

$$\frac{1}{\rho}=\sum_{\alpha=1}^{N}\frac{\omega_\alpha}{\rho_\alpha},\tag{6}$$

where ρ_α is the density of a fluid with $\omega_\alpha = 1$.

With the same assumptions, the PDF equation (2) becomes

$$\rho\tilde{u}\frac{\partial P}{\partial z}+\rho\tilde{v}\frac{\partial P}{\partial r}+\rho\sum_{\alpha=1}^{N}\frac{\partial}{\partial\omega_\alpha}(S_\alpha P)=\frac{1}{r}\frac{\partial}{\partial r}\frac{r\mu}{\sigma_p}\frac{\partial P}{\partial r}-\rho\sum_{\alpha=1}^{N}\frac{\partial}{\partial\omega_\alpha}\left[\frac{\varepsilon C_D}{2k}(\omega_\alpha-\langle\omega_\alpha\rangle)P\right].\tag{7}$$

2.3. von Mises coordinates

It is the standard practice [16] to write equations (4) in terms of the von Mises coordinates, (ψ, z) which automatically satisfies mass conservation

$$\mathrm{d}\psi=\rho\tilde{u}r\,\mathrm{d}r.\tag{8}$$

Equations (4) then become

$$\begin{aligned}
&\frac{\partial\tilde{u}}{\partial z}=\frac{\partial}{\partial\psi}r^2\rho\tilde{u}\mu\frac{\partial\tilde{u}}{\partial\psi},\\
&\frac{\partial k}{\partial z}=\frac{\partial}{\partial\psi}r^2\rho\tilde{u}\mu\frac{\partial k}{\partial\psi}+\mu\rho\tilde{u}r^2\left(\frac{\partial\tilde{u}}{\partial\psi}\right)^2-\frac{\varepsilon}{\tilde{u}},\\
&\frac{\partial\varepsilon}{\partial z}=\frac{\partial}{\partial\psi}r^2\rho\tilde{u}\mu\frac{\partial\varepsilon}{\partial\psi}+\mu C_{\varepsilon_1}\frac{\varepsilon\rho\tilde{u}r^2}{k}\left(\frac{\partial\tilde{u}}{\partial\psi}\right)^2-\frac{C_{\varepsilon_2}\varepsilon^2}{k\tilde{u}}.
\end{aligned}\tag{9}$$

The PDF equation (7) becomes

$$\frac{\partial P}{\partial z}+\frac{1}{\tilde{u}}\sum_{\alpha=1}^{N}\frac{\partial}{\partial\omega_\alpha}(S_\alpha P)=\frac{\partial}{\partial\psi}\left\{\frac{\mu}{\sigma_p}\rho\tilde{u}r^2\frac{\partial P}{\partial\psi}\right\}-\frac{1}{\tilde{u}}\sum_{\alpha=1}^{N}\frac{\partial}{\partial\omega_\alpha}\left[\frac{\varepsilon C_D}{2k}(\omega_\alpha-\langle\omega_\alpha\rangle)P\right]. \tag{10}$$

These equations are simply evolution equations with z playing the role of the time-like coordinate.

3. Numerical Method

3.1. Finite-volume scheme

Equations (9) and (10) contain both advective fluxes (the reaction terms in the PDF equation) and diffusive fluxes. In order to construct a numerical scheme, we discretize physical space with mesh spacing $\Delta\psi$ and compositional space with mesh spacing $\Delta\omega$. For the fluid quantities, we define mean quantities in a cell at $z = z_n$ by

$$q_i^n=\frac{1}{\Delta\psi}\int_{(i-1)\Delta\psi}^{i\Delta\psi}q(\psi,z_n)\,\mathrm{d}\psi, \tag{11}$$

where q is one of ($\tilde{u}$, T, k, ε).

For the PDF, we define a mean value at $z = z_n$ by averaging over both physical and compositional space

$$P_{ij}^n=\frac{1}{\Delta\underline{\omega}\Delta\psi}\int_{(i-1)\Delta\psi}^{i\Delta\psi}\int_j P(\omega_1\cdots\omega_N,\psi,z_n)\,\mathrm{d}\underline{\omega}\,\mathrm{d}\psi, \tag{12}$$

where $\Delta\underline{\omega}$ is the volume of a cell in compositional space and $d\underline{\omega} = d\omega_1 \ldots d\omega_N$. The index j refers to the cell in compositional space over which the integration is performed.

Given the flow variables at $z = z_n$, their values at $z = z_{n+1}$ can be found from an explicit finite-volume approximation to the flow equations (9) of the form

$$q_i^{n+1}=q_i^n+\frac{\Delta z_n}{\Delta\psi}(f_i^r-f_i^l)+\Delta z_n s_i, \tag{13}$$

where f_i^l, f_i^r are approximations to the fluxes at the left/right edges of the ith cell and s_i is an approximation to the source term. Obviously

$$f_i^l=f_{i-1}^r.$$

An approximation that is first order in Δz is obtained, if we use values at z_n to compute the fluxes and source terms. The source terms can be calculated from the mean values in the cell.

In order to compute the fluxes, we need approximations to the flow variables and r at the cell edges. The flow variables can be computed from simple averages

$$q_i^r=\tfrac{1}{2}(q_{i+1}+q_i).(\rho_{i+1}+\rho_i). \tag{14}$$

The radius at the cell edges is obtained using using the trapezoidal rule to integrate (8)

$$r_i^r = \sum_{k=1}^{i} \frac{\Delta\psi}{r_i \rho_i^n \tilde{u}_i^n} \quad \text{with } r_i = \frac{1}{2}(r_i^r + r_{i-1}^r). \tag{15}$$

This gives a simple recurrence relation for the r_i^r .

The flux for a quantity q is then given by

$$f_i^r = (r_i^r)^2 \rho_i^r \tilde{u}_i^r \mu_i^r \frac{(q_{i+1}^n - q_i^n)}{\Delta\psi}, \tag{16}$$

where μ_i^r is calculated from the flow variables at the cell edge. Since this is a central difference approximation to diffusive terms, the resulting scheme is second order in $\Delta\psi$.

The procedure for P is similar, except that we have to include the terms involving gradients in compositional space. Since these are advective, we need to use an upwind difference. With the LMSE approximation, the effective advective velocity in the α direction in the compositional space is

$$\dot{\omega}_\alpha = \frac{1}{\tilde{u}} \left(S_\alpha + \frac{\varepsilon C_D}{2k} (\omega_\alpha - \langle \omega_\alpha \rangle) \right). \tag{17}$$

The PDF is then updated via

$$P_i^{n+1} = P_i^n + (\Delta P)_p + \frac{\Delta z}{\Delta\omega} \sum_{\alpha=1}^{N} [(\dot{\omega}_\alpha P)_i^r - (\dot{\omega}_\alpha P)_i^l], \tag{18}$$

where $(\Delta P)_p$ is the increment due to the diffusive term in physical space. A first-order upwind approximation is obtained by setting the flux at a cell face perpendicular to the α direction to

$$(\dot{\omega}_\alpha P)_i^r = \begin{cases} \dot{\omega}_\alpha P_l^n & \text{for } \dot{\omega}_\alpha > 0, \\ \dot{\omega}_\alpha P_r^n & \text{for } \dot{\omega}_\alpha < 0, \end{cases} \tag{19}$$

where P_l^n and P_r^n are the values in the cells on the left and right of the cell face. Here $\dot{\omega}_\alpha$ is evaluated at the centre of the cell face.

The net result is a scheme that is second order in Δr, but first order in Δz and $\Delta\omega$. In order to make it second order in all variables, we first use the first-order scheme to compute an intermediate solution, $f_i^{n+1/2}$, at the half-step $z_{n+1/2} = (z_n + z_{n+1})/2$. These values are then used to compute the fluxes and source terms for the flow variables, which are used to update them through a complete timestep, i.e.

$$q_i^{n+1} = q_i^n + (\Delta q)_i^{n+1/2}, \tag{20}$$

where $(\Delta q)_i^{n+1/2}$ is computed using the values at the half-step.

The same is done for the flow terms in the PDF equation, but in order to get second-order accuracy in $\Delta\omega$, we need a better approximation to the advective fluxes in the compositional space. This can be obtained by first using the intermediate solution to calculate an average gradient in the α direction from

$$\left(\frac{\partial P}{\partial \omega_\alpha} \right)_i^{n+1/2} = \frac{1}{\Delta\omega_\alpha} av(P_r^{n+1/2} - P_i^{n+1/2}, P_i^{n+1/2} - P_l^{n+1/2}), \tag{21}$$

where *av*(*a*, *b*) is a non-linear averaging function and the subscripts *l*, *r* denote values in the neighbouring cells on the left and right in the α direction. It is essential to use a non-linear averaging function here because Godunov's theorem [17] tells us that a scheme that is second order everywhere will generate oscillations, where the solution changes rapidly. This applies in this case if the PDF approaches a delta-function, but if it is smooth then one can use a simple average.

The gradients given by Equation (21) are then used to obtain a better approximation to *f* at a cell face. For example, for a face perpendicular to the α direction, the values of f_l and f_r to be used in (19) are given by

$$P_l = P_i^{n+1/2} + \frac{\Delta\omega}{2}\left(\frac{\partial P}{\partial \omega_\alpha}\right)_i^{n+1/2}$$
$$P_r = P_j^{n+1/2} - \frac{\Delta\omega}{2}\left(\frac{\partial P}{\partial \omega_\alpha}\right)_j^{n+1/2}, \qquad (22)$$

where *i* and *j* are the cells on the left and right of the face. The final solution at $z = z_{n+1}$ is then obtained from Equation (18) using these values of P_l and P_r. This is essentially the same scheme as that described in [18] for compressible flow. Although it is not as accurate as some schemes for linear advection, it is robust and simple to implement.

3.2. Adaptive mesh refinement

Unlike most AMR codes, e.g. [8–12], in this study refinement is on a cell-by-cell basis instead of being organized into patches. This provides a more efficient grid at some increased cost of integration. Figure 1 shows how this works in two dimensions for a thin region, such as a shear layer, that requires high resolution.

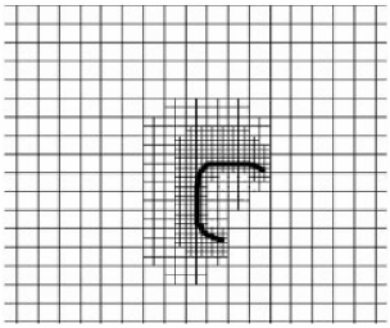

Figure 1. Grid refinement at a region requiring high resolution (represented by thick black curve).

We use a hierarchy of uniform grids $G_0 \ldots G_L$ so that if the mesh spacings on G_0 are $(\Delta\psi, \Delta\omega)$, then they are $(\Delta\psi/2^n, \Delta\omega/2^n)$ on G_n. Grids G_0 and G_1 cover the whole computational domain, but the finer grids need only exist in regions that require high resolution. The grid hierarchy is used to generate an estimate of the relative error by comparing solutions on grids with different mesh spacings and the grid refines if this error exceeds a tolerance E_r and derefines if it is less than E_d. Refinement also occurs in *z* so that if the step on G_0 is Δz, then it is $\Delta z/2^n$ on G_n.

The integration algorithm is recursive and is described by a pseudo-code for integration of grid G_n over its *z* step. From the pseudo-code given below, the procedure *integrate(0)* performs integration on all grids through one G_0 grid *z*-step, Δz. This process is shown schematically in Figure 2 for four grid levels. From the figure it can be seen that a coarse grid solution at the

advanced time is available whenever a fine grid is integrated. This coarse grid solution provides a space-time interpolant that is used to impose the boundary conditions on the fine grid at a coarse-fine grid boundary.

```
procedure integrate(n){                 Integrate G_n
   step(n)                              Advance G_n by one timestep Δt/2^(n-1)
      if(n<N−1){                        Finer grids exist
         while (t_n<t_(n−1)){
              integrate(n+1)            Integrate G_(n+1) to G_n time
               t_n = t_n + Δt/2^n       Increment G_n time by Δt/2^L
         }                              end of while loop
         regrid(n)                      Compare solutions on G_n and
                                        G_(n−1) → decide G_(n+1) refinement
         merge(n)                       Project G_(n+1) solution onto G_n
      }                                 end of if block
return
}                                       end of procedure integrate(n)
```

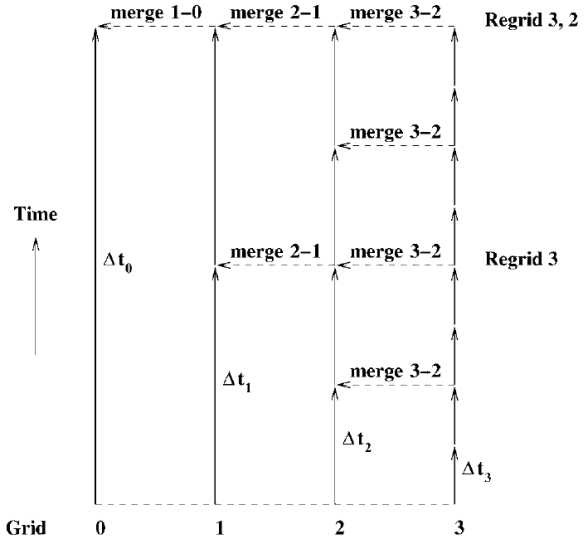

Figure 2. Integration of a four-level grid.

In the *merge(n)* operation, the solution in the cells on G_n that are refined is replaced by the volume average of the solutions in the G_{n+1} cells that it contains. This ensures that the solutions on all grids are consistent.

The simplest way to apply AMR to this system would be to treat it as a problem in N+1 dimensions (r and the N dimensions in compositional space). However, this would mean that if a cell is refined in one dimension, then it is also refined in all the others. This would not be very efficient since there is no reason why physical and compositional space should both be refined at the same place. For example, near the centreline of a jet, there might very little variation with r, but P could be very close to a delta-function, which would require a high degree of refinement in the compositional space.

In order to allow different levels of refinement in the physical and compositional space, we associate a complete compositional space hierarchy with each physical cell on every grid level. The number of levels of refinement of the compositional space in a particular physical cell is then determined by the accuracy requirements for that particular cell. So, for example, the maximum number of grid levels will be used in compositional space if P is close to a delta-function, whereas a smaller number of levels will be used if it is smooth.

4. Verification and Validation

It is obviously important to demonstrate that the code described does indeed solve the equations accurately. In our previous paper [4] in which there was no space dependence, we were able to compare the results both with the analytic solutions and the Monte Carlo calculations. This is not possible in this case because there are no non-trivial analytic solutions for the complete problem described, and it is impossible to compare with Monte Carlo solutions on a like-for-like basis given that the current method uses the AMR in both physical and compositional space.

However, it is possible to verify that the code does provide an accurate solution to both the flow equations and the PDF equation. As far as the flow equations are concerned, these are exactly the same as those implemented in previous work [19] in the GENMIX package [16], except that we assume the pressure to be constant. The latter implementation is also based on the solution of conservation equations for the mean and variance of mixture fraction, rather than deriving such values from a transported PDF. We can therefore use this implementation within GENMIX to check our results. Since we are using a different numerical scheme, agreement would indicate that both our schemes and its implementation are correct for this part of the problem. Agreement would also indicate that our assumption of constant pressure is reasonable for these flows.

As for the PDF, we have already shown that our scheme is accurate for a PDF with no space dependence [4]. The space-dependent term in the PDF equation is simply a diffusion term, which we can check against simple analytic solutions by setting all other terms in the PDF equation to zero.

The final check is to ensure that the rather complicated AMR procedure is reliable. This can be done by simply comparing the AMR solution with a high-resolution calculation on a uniform grid.

4.1. Flow solver test

For this test, we consider the mixing of a single passive scalar in a non-reacting jet. We compare our results with those derived on the basis of the GENMIX implementation and with the experimental data of Schefer and Dibble [20], who studied a non-reacting propane jet in a co-flowing stream of air. The parameters of the problem are given in Table I. Figure 3 shows that our AMR calculation agrees well with both previous [19] GENMIX results and the available data. Only small differences are observed between the two sets of predictions for the mean mixture fraction, although some slight differences do occur for the variance of the mixture fraction fluctuations. These are, however, likely due to differences in the way this quantity was determined, i.e. in one case from the direct solution of a conservation equation and in the second from the transported PDF itself. Overall, however, the comparisons serve to verify that the flow solver is in line with the previous predictions and experimental data.

Table I. Parameters for the calculations.

Turbulence model constants	$C_\mu = 0.09$, $C_{\varepsilon 1} = 1.44$, $C_{\varepsilon 2} = 1.92$, $C_D = 4$, $\sigma_k = 1$, $\sigma_\varepsilon = 1.3$, $\sigma_p = 1$
Nozzle diameter	0.00526 m
Jet density	1.8638 kgm^{-3}
Co-flow density	1. 1964 kg m^{-3}
Initial jet velocity	1/7 law with $\tilde{u}$ = 69.89 ms^{-1} on centreline
Width of computational domain	10 nozzle diameter

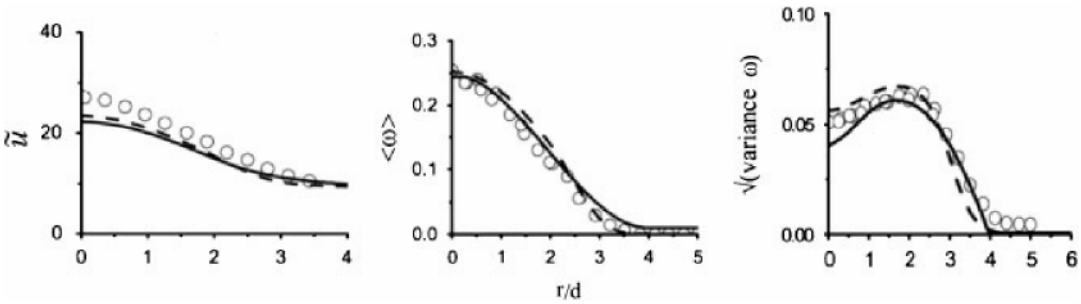

Figure 3. Flow variables at z = 30 diameters: dashed line – GENMIX with 200 mesh points in the ψ direction; solid line – AMR using a resolution of five levels of refinement with 30 coarse cells across the width of the physical space, and five levels of refinement with 25 coarse cells for each associated compositional space; symbols – experimental results from Scheffer and Dibble [20].

4.2. Diffusion test for PDF

In order to test the correct implementation of the spatial diffusion term in the PDF equation, we consider a simple problem for which an analytic solution is available. The flow variables are set to be constant throughout with

$\tilde{u}$ = 70 ms^{-1}, v = 0.0, k = 12.25 m^{2}s^{-2} , ε = 38267.6 m^{2}s^{-3}.

These values are typical of those found in the full calculation considered previously. The resolution involved four levels of refinement, with 25 and 30 coarse cells for the compositional and physical spaces, respectively. The PDF at the nozzle exit is a delta-function in compositional space located at the mean. The mean is initially a Gaussian with

$$\langle P\rangle = \exp(-r^2/\sigma_0^2).$$

With these assumptions, Equation (7) becomes

$$\frac{\partial\langle P\rangle}{\partial z} = \frac{D}{r}\frac{\partial}{\partial r}r\frac{\partial\langle P\rangle}{\partial r},$$

with

$$D = \frac{\mu}{\sigma_p \rho u}$$

The fundamental solution of the above diffusion equation in two dimensions then tells us that the solution at z is

$$\langle P\rangle = \frac{z_0}{(z_0+z)}\exp\left[-\frac{r^2 z_0}{\sigma_0^2(z_0+z)}\right],$$

where

$$z_0 = \frac{\sigma_0^2}{4D}.$$

One can see from Figure 4 that the scheme reproduces the exact solution extremely well.

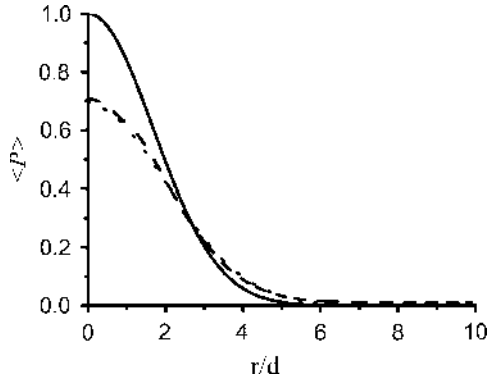

Figure 4. Comparison between the exact solution – dashed line, and the AMR – dotted line, for the simple diffusion test at z = 800 diameters (Note: solid line is the initial distribution of ⟨P⟩ at z = 0).

4.3. AMR test

As already noted, the simplest way to test implementation of the AMR is to compare it with a uniform grid calculation with a resolution equal to that on the finest grid. Results derived in this way, for the case of the mixing of a single passive scalar in a non-reacting jet taken at z/d = 15, are given in Figure 5. It is noted that excellent agreement between the two calculations is observed. The resolution used here for the AMR was five levels of refinement in both compositional and physical spaces, with 25 and 30 coarse cells in each respective space. For the uniform case, the cells were 480 and 400 cells for the compositional and physical spaces, respectively.

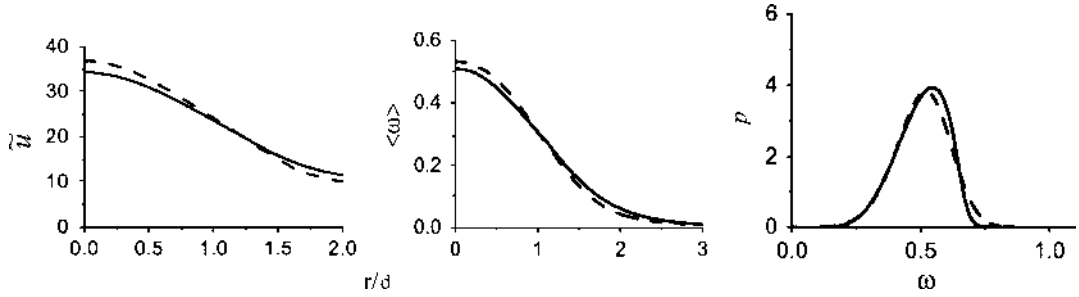

Figure 5. Comparison between the AMR and the uniform calculations for the test case at z = 15 diameters. AMR – solid line and uniform grid – dashed line.

4.4. Reacting flow

It is clear that our method is of little practical interest unless it is capable of handling reacting flows. In order to demonstrate this, we consider the same flow as in Section 4.1, with the jet consisting of pure fuel (ω_1) and the co-flow of oxidant (ω_1). These react according to the simple temperature-independent kinetics

$$S_1 = -\omega_1\omega_2, \quad S_2 = -S_1. \tag{23}$$

There are no analytic solutions or appropriate experimental results with which we can compare this solution. However, it can be demonstrated that the code gives reasonable results and that it achieves numerical convergence without excessive computational cost.

From Figure 6 it can be seen that with a sufficient number of refinement levels, the AMR agrees very well with a numerically converged solution on a uniform grid.

The model run times shown in Table II provide an idea of the reduction in computing time obtained with the AMR for a numerically converged solution. In our previous paper [4], we showed that the computational cost is considerably reduced when the PDF only differs

significantly from zero in a small part of compositional space. In this case, the reduction in computing time is even greater because, as can be seen from Figure 7, high resolution is not required in all parts of physical space. Note that these results also show why it is essential to have different levels of refinement in physical and compositional space. For example, in the far-downstream region the solution in the jet is smooth in physical space, but is close to a delta-function in compositional space.

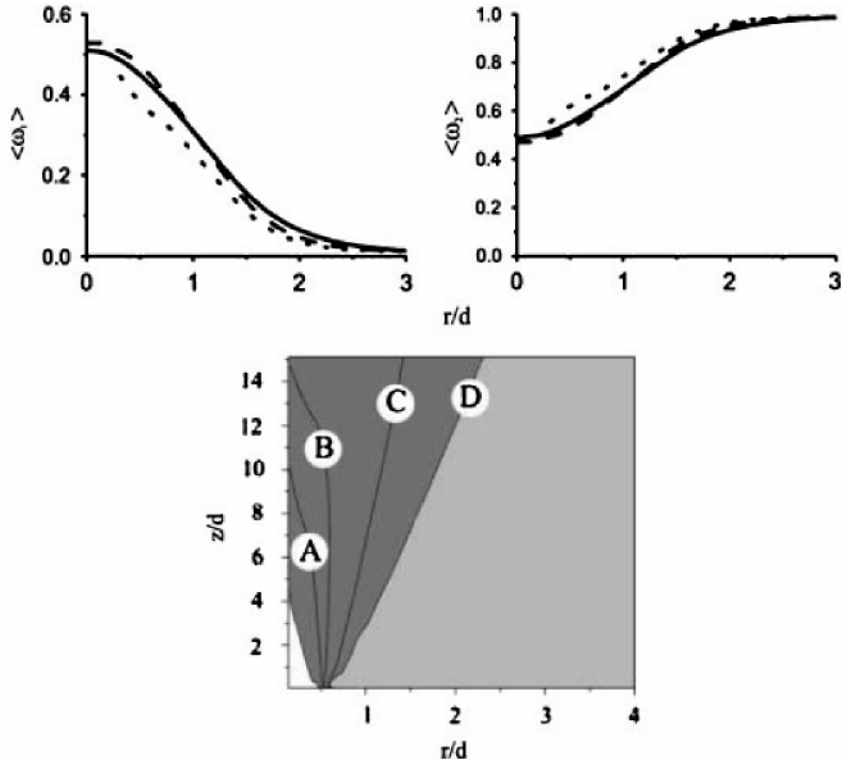

Figure 6. Comparison between the AMR and the uniform grid calculation for the reacting case of $\omega_1 \rightarrow \omega_2$ at z =15 diameters. AMR – dotted line three levels and dashed line four levels of refinement (30 coarse physical cells with 25^2 coarse compositional cells); uniform grid – solid line (240 physical cells and 200^2 compositional cells). Below a flow field map is shown: white region – wert potential core, dark grey region – shear layer, light grey region – coflow. Contour lines shown in the shear layer are of constant mass fraction (A=0.753; B =0.522; C=0.150 and D=0.025).

Table II. Comparison of run times between the AMR at different levels of refinement and a numerically converged solution on a uniform grid for the reactive test case with two species. Runs were performed on a Dual Intel Xeon E5440 base (2.83 GHz, 1333FSB, 26 MB, Quad core) with 64GB, 667 MHz, ECC Memory (164 GB).

Type	Physical cells	Sample cells	CPU time (*s*)	Distance downstream *z/d*	Computer memory (GB)	AMR CPU speed-up
Uniform	240 (1 level)	200^2 (1 level)	2266791	15.0	60.00	-
AMR	30 (coarse) (4 levels)	25^2 (coarse) (4 levels)	54723	15.0	3.54	41.4
AMR	30 (coarse) (3 levels)	25^2 (coarse) (3 levels)	13755	15.0	0.91	-

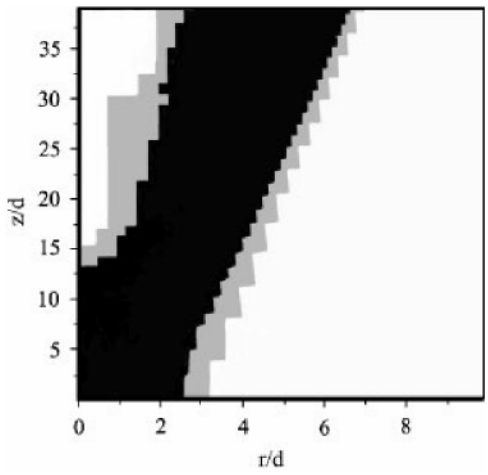

Figure 7. Map of grid-adaptative refinement. The white areas show grid level G_1, grey G_2 and black G_3.

5. Conclusions

A novel solution method for the scalar transported PDF equation has been described. In contrast to conventional solution methods that employ Monte Carlo methods, this study is based on a finite-volume scheme combined with an AMR approach in both the physical and compositional space. We have carried out a number of test calculations involving simple mixing and reacting flows in which the flow turbulence is described by the standard k-ε model. These show that the use of AMR can give high accuracy at a fraction of the cost of uniform grids.

On the basis of these results and those in our previous paper [4] one can conclude that finite-volume schemes with the AMR provide an attractive alternative to the Monte Carlo-based methods. However, accuracy requirements dictate that neither method is viable for very large numbers of scalars.

Ackowledgements

The authors thank the Engineering and Physical Sciences Research Council for their financial support of this work reported in this paper.

References

1. Pope SB. PDF methods for turbulent reactive flows. *Progress in Energy and Combustion Science* 1985; **11**: 119-192.
2. Janicka J, Kolbe W, Kollmann W. Closure of transport equation for the probability density function of turbulent scalar fields. *Journal of Non-Equilibrium Thermodynamics* 1979; **4**:47-66.
3. Sabel'nikov V, Soulard O. Rapidly decorrelating velocity-field model as a tool for solving one-point Fokker-Planck equations for probability density functions of turbulent reactive scalars. *Physical Review E* 2005; **72**: 16301-163022.
4. Olivieri DA, Fairweather M, Falle SAEG. An adaptive mesh refinement method for solution of the transported PDF equation. *International Journal for Numerical Methods in Engineering* 2009; **79**:1536-1556.
5. Maas U, Pope SB. Simplifying chemical kinetics: intrinsic low-dimensional manifolds in composition space. *Combustion and Flame* 1992; **88**:239-264.
6. Huang H, Fairweather M, Griffiths JF, Tomlin AS, Brad RB. A systematic lumping approach for the reduction of comprehensive kinetic models. *Proceedings of the Combustion Institute* 2005; **30**:1309-1316.
7. Goussis DH, Lam SH. A study of homogenous methanol oxidation kinetics using CSP. *Proceedings of the Combustion Institute* 1992; **24**:113-120.

8. Berger MJ, Oliger J. Adaptive mesh refinement for hyperbolic partial differential equations. *Journal of Computational Physics* 1984; **53**:484-512.
9. Berger MJ, Colella P. Local adaptive mesh refinement for shock hydrodynamics. *Journal of Computational Physics* 1989; **82**:64-84.
10. Bell J, Berger M, Saltzmann J, Welcome M. Three dimensional adaptive mesh refinement for hyperbolic conservation laws. *Society for Industrial and Applied Mathematics Journal on Scientific Computing* 1994; **15**:127-138.
11. Quirk JJ. A parallel adaptive grid algorithm for computational shock hydrodynamics. *Applied Numerical Mathematics* 1996; **20**:427-453.
12. Baum JD, L¨ohner R. Numerical simulation of shock-elevated box interaction using an adaptive finite shock capturing scheme. *American Institute of Aeronautics and Astronautics* 1989; AIAA-1989-653.
13. Curl RL. Dispersed phase mixing: 1 theory and effects in simple reactors. *American Institute of Chemical Engineers Journal* 1963; **9**:175-181.
14. Dopazo C. Relaxation of initial probability density functions in turbulent convection of scalar fields. *Physics of Fluids* 1979; **22**:20-30.
15. Jones WP, Kakhi M. PDF modelling of finite-rate chemistry effects in turbulent nonpremixed jet flames. *Combustion and Flame* 1998; **115**:210-229.
16. Spalding DB. GENMIX: *A General Computer Program for Two-Dimensional Parabolic Phenomena*. Pergamon Press: Oxford, 1977, ISBN: 0-08-021708-7.
17. Godunov SK. Finite difference methods for numerical computations of discontinuous solutions of the equations of fluid dynamics. *Matematicheski Sbornik* 1959; **47**:271-306.
18. Falle SAEG. Self-similar jets. *Monthly Notices of the Royal Astronomical Society* 1991; **250**:581-596.
19. Alvani RF, Fairweather M. Modelling of the ignition characteristics of flammable jets using a k-ε-γ turbulence model. *Proceedings of 4th International Symposium on Turbulence, Heat Mass Transfer*, Hanjalic K, Nagano Y, Tummers MJ (eds). Begell House Inc.: New York, 2003; 911-918.
20. Schefer RW, Dibble RW. Mixture fraction field in a turbulent non-reacting propane jet. *American Institute of Aeronautics and Astronautics Journal* 2001; **39**:64-72.